



The development of the Scaled Accelerated Loading Simulator facility and transfer functions to the full-scale pavement using theory of similitude by finite element analysis

Shih-Hsien Yang^{a,*}, Chien-Wei Huang^b, Yi-Ning Sun^c, Hery Awan Susanto^a

^a Department of Civil Engineering, National Cheng Kung University, Tainan 70101, Taiwan

^b Department of Civil Engineering, National Chung Hsing University, Taichung 40227, Taiwan

^c Simutech Solution Corp., Taipei 10406, Taiwan

Received 8 September 2017; received in revised form 21 March 2018; accepted 22 March 2018

Abstract

The purpose of this study is to investigate the relationship of the vertical deformation between the scaled-down pavement test and full-scale pavement structure according to the theory of similitude-based analysis procedure. Finite element analysis used to investigate and establish the relationship between the scaled-down and full-scale models. Four scaled-down models with scaling factors of 0.9, 0.75, 0.6, and 0.45 with two types of constitutive models of asphalt concrete materials, elastic and viscoelastic, are considered. The results show that the vertical deformation in the full-scale model achieved by applying a vertical shift to the vertical deformation in the scaled-down model. The vertical shift factor varies linearly in normal and logarithm scale with the scaling factor from 0.9 to 0.45 for linear elastic and viscoelastic material, respectively. Moreover, this study proposes a systematic analysis procedure to determine the testing temperature in the SALS test at a specific loading speed by using the time–temperature superposition principle. This study contributes considerably to preliminary understanding of the relationship between the scaled-down tester in the laboratory and the full-scale model according to the theory of similitude.

© 2018 Chinese Society of Pavement Engineering. This is an open access article under the CC BY-NC-ND license (<http://creativecommons.org/licenses/by-nc-nd/4.0/>).

Keywords: The theory of similitude; APT (Accelerated Pavement Testing); SALS (Scaled Accelerated Loading Simulator); Finite element analysis; Viscoelastic; Scaled-down model

1. Introduction

Accelerated Pavement Testing (APT) [1] is a useful tool for evaluating long-term pavement performance in laboratory testing. Full-scale APT involves the controlled application of a prototype wheel load to a prototype

pavement system to determine pavement response and performance for an accelerated accumulation of damage in a compressed period. Full-scale APT facilities have been developed to simulate the service conditions of pavement in the field. Such facilities apply load and tire pressures equal to the load experienced by the pavement in the field. These pressures are adjustable to apply a wide range of loads experienced by the pavement in the field. Usually, a test section or several test sections are prepared using one or several mixes, and the full-scale load is applied continuously until test sections of the pavement fails. The test sections are generally instrumented with strain gauges and pressure sensors, and continuous data acquisition is

* Corresponding author.

E-mail addresses: shyang@mail.ncku.edu.tw (S.-H. Yang), stanhuang917@nchu.edu.tw (C.-W. Huang), nina@simutech.com.tw (Y.-N. Sun), N68047018@ncku.edu.tw (H.A. Susanto).

Peer review under responsibility of Chinese Society of Pavement Engineering.

performed. The data acquired are later analyzed for determining pavement performance, for example, in terms of fatigue and rutting characteristics. For many years, pavement engineers have successfully used accelerated full-scale pavement testing to evaluate material and pavement performance for developing and verifying design procedures.

Heavy vehicle simulators (HVSs), which are full-scale loading equipment, apply load and tire pressures equal to the load experienced by the pavement in the field. Harvey et al. discussed the results obtained from HVS tests which evaluated the fatigue performance of asphalt concrete mixes and influence of several parameters, such as mix proportions and air void contents, on the fatigue life of asphalt concrete. The designated thickness of hot mixed asphalt (HMA) was adequate in terms of permanent deformation performance but inadequate in terms of fatigue performance [2]. In 1991, the linear facility LINTRACK [3] was developed by the Road and Railroads Research Laboratory at the Delft University of Technology. Groenendijk et al. investigated the performance of 150- and 70-mm-thick HMA pavements in the field using LINTRACK. The behavior of the strain gauges under the LINTRACK wheel track was reported, and the measured strain distribution showed that the magnitude of transverse strains was higher than that of the longitudinal strains. Moreover, the study reported that temperature corrections are necessary to account for strains arising from temperature variation during the test [3]. The Texas Mobile Load Simulator (TxMLS), launched in 1995, was used in the TxMLS program in Texas to investigate the load damage equivalency and remaining life of a field pavement [4]. Hugo et al. [4] presented an overview of the program and discussed two rehab strategies developed for the TxMLS in 1995 and 1996. The findings provided conclusive results on the relative performance of the rehab strategies and learning acquired during the test program. The study concluded that pavement rutting was contributed to by the effects of temperature, material properties, pavement structure, and applied load. The total rutting occurred mainly in the top rehab layer and immediately in the original sublayer.

The value of performing full-scale pavement testing is without a doubt; however, it is very costly to maintain and operate the system. Thus, one of the alternative means is to use scaled-down APT devices such as the Model Mobile Load Simulator (MMLS), which can be used to investigate asphalt mixture behavior under a repeated scaled traffic load [5,6]. The MMLS and MMLS3 are 1:10 and 1:3 scaled-down APT devices, respectively, for use in a controlled environmental chamber. They are used for testing pavements in the laboratory with scaled-down structures. The MMLS was originally developed as a demonstration model for the TxMLS and was later mechanized for 1:10 APT. The MMLS comprises loading equipment and a mold for preparing a scaled model of pavement. The mold has a size of $3000 \times 1100 \times 20 \text{ mm}^3$. The loading device uses a wheel load of 200 N with double

bogie and solid 25-mm-wide tire. It has a maximum velocity of 1.1 m/s and can provide 10,000 passes per hour of the unidirectional wheel load. It was concluded that the MMLS 1:10 model can be successfully used for investigating the structure response for various loading parameters, provided appropriate scaling was performed. However, many practical difficulties were experienced when scaling down the material properties and thickness of the model pavement layers by 1:10 [5]. To overcome some of the scaling constraints experienced and facilitate a wider spectrum of applications, a new model of the device using a 1:3 scale of the full-scale pavement geometry and load was developed. This model, the MMLS3, has been used successfully in the field to monitor the rutting and fatigue potential of mixes. This device comprises a larger mold and loading equipment. It can be used in the field by placing it directly on pavements or in the laboratory on a model scaled layered pavement structure of $2744 \times 915 \times 305 \text{ mm}^3$. The loading equipment has four bogies, one axle per bogie, and one wheel per axle. It has four tires, each 80-mm wide, with maximum inflatable pressure of 800 kPa, and axle load of 1.9–2.7 kN. The nominal wheel load application rate is 7200 single-wheel load repetitions per hours (7200 swlr/h) at a nominal speed of 2.5 m/s [7].

However, for a scaled-down structure, the validity of the test is a concern. The theory of similitude provides a scaling principle for determining variables such as material properties, geometries, model parameters, and testing configuration in a scaled-down model; the response of the scaled-down test is comparable with that of the full-scaled test. This theory is extensively utilized in structural engineering to solve the scaling problem. Simitse and Rezaeepazhand et al. investigated the structural response of the flat laminated plates subjected to transverse loads, buckling, and free vibration [8–10]. Ramu et al. extensively deduced the physical phenomena such as the cantilever beam subjected to a transverse point load and the flat elastic plate with free transverse vibrations [11]. In terms of the application of the theory of similitude in pavement engineering, Bhattacharjee et al. (2004) performed a 3D static finite element analysis (FEA) to investigate the stress–strain behavior in the MMLS3 test. The study concluded that the finite element model of MMLS3 successfully described the behavior of MMLS3 observed in laboratory in terms of effect of variation of pavement thickness and relative magnitude of strains in different directions [12]. Although the Scaled Accelerated Loading facilities have already widely used to evaluate the pavement and material performance in pavement engineering, few studies have examined the application of the theory of similitude in pavement engineering.

Therefore, the objective of this study is to investigate the relationship of the vertical deformation between the scaled-down pavement structure and full-scale pavement structure under tire loading according to the theory of similitude-based analysis procedure using FEA. First, the theory of similitude is introduced and validated for a two-layer structural system. Full-scale and scaled-down FE models are

constructed and the numerical results of vertical deformation, octahedral stresses and strains were compared between two FE models to conduct the validation of the theory of similitude. Second, full-scale and scaled-down FE models are developed for field pavement structures and Scaled Accelerated Loading Simulator (SALS) facilities, respectively. The vertical deformation of the full-scale and scaled-down models is compared, and the transfer functions (δ) for vertical deformation between scaled-down and full-scale model can be developed. To conduct a preliminary investigation of material effect on scaling problem, this study considers asphalt concrete as homogeneously elastic and time-temperature dependent viscoelastic material. Third, this paper proposes a procedure for determining the optimal testing temperature according to the time-temperature superposition principle.

2. Theory of similitude and FE verification

In this section, the concept and derivation of the theory of similitude was first presented and scaled-down and full-scaled finite element pavement models were constructed based on the principle of similitude. The responses from both models were used to verify the theory of similitude.

2.1. Theory of similitude

Scaled down models are widely used for experimental investigations of huge structures because of the limitation in the capacities of testing facilities and the efficiency of experiment. To achieve this goal, the concept of similitude is often used so that measurements made one system in the laboratory environment (scaled-down model) can be used to describe the behavior of other similar system in field (full-scale model). Construction of a scaled-down model, however, must be accompanied by an analysis to determine what conditions it is tested under. According to the theory of similitude, all fundamental physical variables, such as length, time, and mass, can be expressed in dimensionless form, and other variables can be derived and reproduced at exactly the same proportions in the scaled-down model as in the full-scale model. The Buckingham π theorem was introduced for dimensional analysis in the theory of similitude. According to the Buckingham π theory, the physical variables in the dimensional domain can be expressed as Eq. (1), whereas all variables can be transferred in the dimensionless π domain shown in Eq. (2).

$$F(x_1, x_2, x_3, \dots, x_n) = 0 \tag{1}$$

$$G(\pi_1, \pi_2, \pi_3, \dots, \pi_{n-r}) = 0 \tag{2}$$

where F is the physical domain in the dimensional form, G represents the dimensionless π domain based on the Buckingham π theorem, x_i represents the i^{th} physical variables, π_i represents the dimensionless physical variables, n is the total number of physical variables, and r is the number of fundamental variables. In the dimensionless π domain,

the physical variables are reduced from n to $n - r$ terms using the dependency of dimensions.

For the mechanical problem, the most common physical variables are geometric parameter (H), material modulus (M), loading force (F), deformation variable (U), stress (σ) and strain (ε) as shown in Eq. (3).

$$F(H, M, F, U, \sigma, \varepsilon) = 0 \tag{3}$$

In Eq. (3), because the selected fundamental variables must be independent from other variables, the fundamental variables H and M are selected as fundamental variables in this research. The dependent variables such as F , U , σ and ε can be represented by fundamental variables H and M shown as Eqs. (4)–(7). Thus, the dependent variables in dimensionless domain G can be shown as Eq. (8).

$$F \rightarrow MH^2 \tag{4}$$

$$U \rightarrow H \tag{5}$$

$$\sigma \rightarrow M \tag{6}$$

$$\varepsilon \rightarrow 1 \tag{7}$$

$$G(F, U, \sigma, \varepsilon) \rightarrow G\left(\frac{F}{MH^2}, \frac{U}{H}, \frac{\sigma}{M}, \varepsilon\right) = 0 \tag{8}$$

In Eq. (7), since the strain in dimension domain F is already dimensionless, the strain term in dimensionless domain G is as same as it in dimension domain. The dimensionless domain G of scaled-down and full-scale model can be formed as Eqs. (9) and (10), respectively.

$$G_S(\pi_{S1}, \pi_{S2}, \pi_{S3}, \pi_{S4}) = G_S\left(\frac{F_S}{H_S^2 M_S}, \frac{U_S}{H_S}, \frac{\sigma_S}{M_S}, \varepsilon_S\right) = 0 \tag{9}$$

$$G_F(\pi_{F1}, \pi_{F2}, \pi_{F3}, \pi_{F4}) = G_F\left(\frac{F_F}{H_F^2 M_F}, \frac{U_F}{H_F}, \frac{\sigma_F}{M_F}, \varepsilon_F\right) = 0 \tag{10}$$

where subscripts S and F indicate the scaled-down and full-scale model in dimensionless domain, respectively. According to the Buckingham π theory, the dimensionless terms π_i must be equal between the scale-down and full-scale dimensionless domain such as $\pi_{Si} = \pi_{Fi}$. The equations of each π terms are shown in Eqs. (11)–(14).

$$\pi_{S1} = \pi_{F1} \rightarrow \frac{F_S}{H_S^2 M_S} = \frac{F_F}{H_F^2 M_F} \tag{11}$$

$$\pi_{S2} = \pi_{F2} \rightarrow \frac{U_S}{H_S} = \frac{U_F}{H_F} \tag{12}$$

$$\pi_{S3} = \pi_{F3} \rightarrow \frac{\sigma_S}{M_S} = \frac{\sigma_F}{M_F} \tag{13}$$

$$\pi_{S4} = \pi_{F4} \rightarrow \varepsilon_S = \varepsilon_F \tag{14}$$

From Eq. (11), the relationship between F_S and F_F can be derived shown as Eq. (15).

$$F_S = \frac{H_S^2 M_S}{H_F^2 M_F} F_F \tag{15}$$

Assuming that the scaling factor of geometric parameter (H) between the scaled-down and full-scale models is N , and the same material properties (M) are used in scaled-down and full-scale model. The Eq. (15) can be yield as:

$$F_S = N^2 F_F \tag{16}$$

where $N = \frac{H_S}{H_F}$ and $\frac{M_S}{M_F} = 1$. Similarly, the relationship between the full-scale and scaled-down models of the deformation, stress and strain can be derived shown as Eq. (17).

$$\begin{aligned} U_S &= \frac{H_S}{H_F} U_F = N U_F; \\ \sigma_S &= \frac{M_S}{M_F} \sigma_F = \sigma_F \text{ and} \\ \varepsilon_S &= \varepsilon_F \end{aligned} \tag{17}$$

The relationships of all involved physical phenomena are summarized in Table 1.

2.2. Verification of the theory of similitude

To verify the theory of similitude, the full-scale and scaled-down models are compared using FEA. Two 3D FE models are constructed using commercial software ABAQUS to represent the full-scale and scaled-down sections. The FE analysis domain in length and width are both

1000 mm for scaled-down and full-scale model. Thus, length and width dimensions were kept the same between two models. The full-scale model comprises two layers of 100 mm thickness, whereas the scaled-down model with scaling ratio $N = 0.6$ comprises two layers of 60 mm thickness. An identical loading pressure of 690 kPa is applied to the center of the surface. The element size is $1 \text{ mm} \times 1 \text{ mm} \times 1 \text{ mm}$ for scaled-down and full-scale FE model. The material properties for each layer are shown in Fig. 1. The comparison of stress and vertical deformation between the full-scale and scaled-down models is evaluated to verify the theory of similitude. Fig. 2 shows the vertical deformation U_3 contours of the full-scale and scaled-down FE models. In order to compare the response between scaled-down and full-scale model in three-dimension domain, this research employ the octahedral invariant for stress and strain. In terms of the octahedral normal and shear strains of the models shown in Fig. 3, the behavior of the two models is comparable along with the normalized depth. According to the theory of similitude, if the models are subjected to the same level of loading pressure, both models should have the same strain responses. These results confirm the conclusion of the theory. Fig. 4 shows the comparison results of the octahedral normal and shear stresses for the full-scale and scaled-down models. The results show that the octahedral stresses within the full-scale model coincide with the stresses within the scaled-down model. These results validate the conclusion of the theory of similitude between the full-scale and scaled-down models for a two-layer system.

In most engineering applications, complete similitude may be impossible for every engineering variable [13]. However, the use of the scaled-down model can still be valid for the measured variables if the improperly scaled variables do not exert a marked effect on the measured variables. Because SALS are designed for evaluating rutting, this study uses vertical deformation (U_3) as the measured variable. Moreover, the pavement structure is a multilayer system generally comprising the asphalt, base,

Table 1 Relationships of physical phenomena of the two-layer pavement system.

Physical phenomenon	Relationship ($F:S$)
Geometric variable (H)	1: N
Material modulus (M)	1:1
Loading force (F)	1: N^2
Deformation (U)	1: N
Stress (σ)	1:1
Strain (ε)	1:1

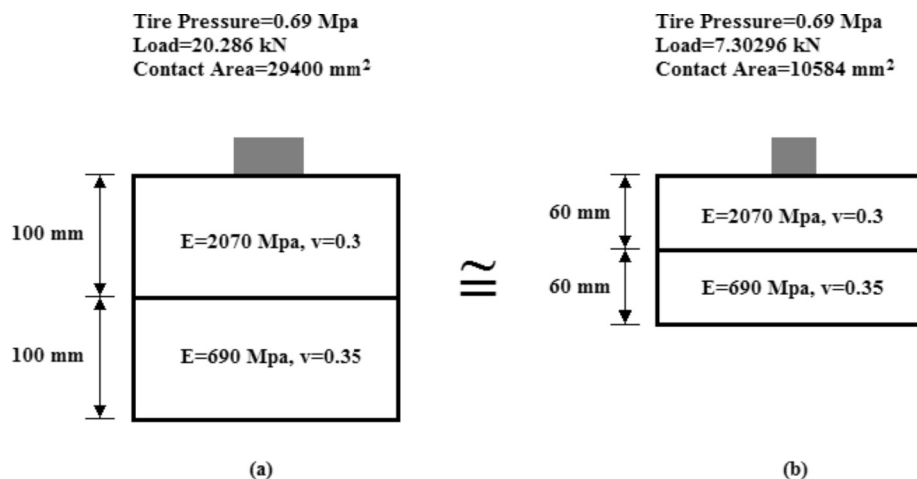


Fig. 1. Finite element configurations of the (a) full-scale and (b) scaled-down models.

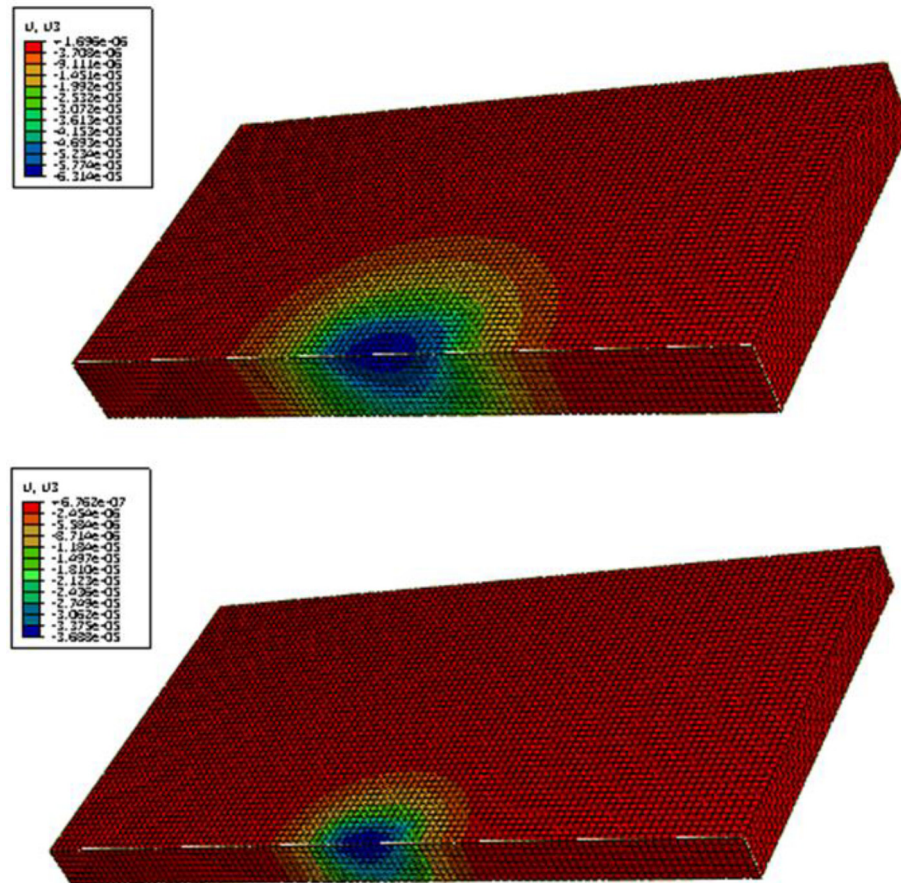


Fig. 2. Contours of the (a) full-scale and (b) scaled-down models.

subbase, and subgrade layers. Because it is not easy to develop a SALS device with same multilayer system of real pavement structure in the laboratory, the SALS device in this research is designed as a two-layer structure system with asphalt and neoprene layers. Moreover, the thickness of asphalt layer and loading pressure is scaled down for the SALS facility based on the theory of similitude. The FEA with different scaled-down ratio N will be conducted, and the transfer functions (δ) between the full-scale and scaled-down models can be determined on the same basis of the material properties and the thickness of the neoprene layer.

3. Development of SALS configuration according to the theory of similitude

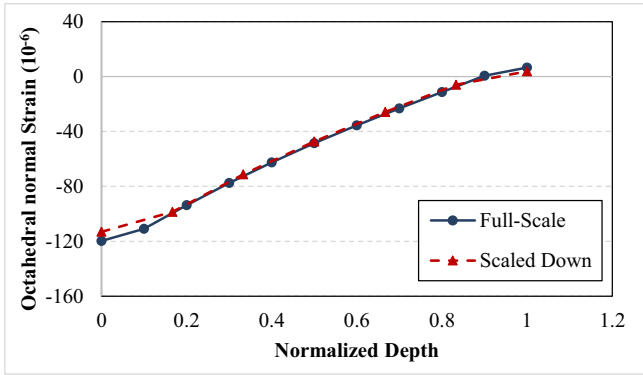
This section presents an analytical approach to developing the relationship between the full-scale pavement and SALS device according to the theory of similitude. The commercial FE software ABAQUS is employed to construct the full-scale and SALS FE models. The full-scale pavement model is considered a four-layer system, whereas the SALS model comprises two layers. Two properties of the asphalt layer material, elasticity and viscoelasticity, are considered in analyzing the effect of different asphalt materials. Subsequently, the SALS testing temperature

and loading speed according to the time–temperature superposition principle are determined.

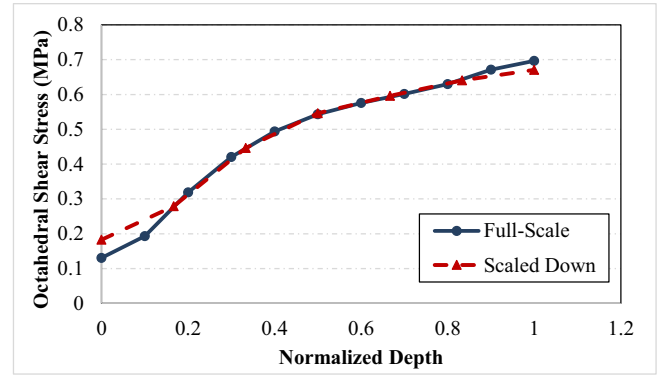
This study uses FEA to simulate structural responses and compare the calculated results to determine the accuracy of the SALS facility compared with the full-scale model. The full-scale FE model is constructed to represent the actual pavement structure; moreover, the SALS FE model is developed according to the geometry and boundary condition of the SALS facility.

3.1. Full-scale FE model

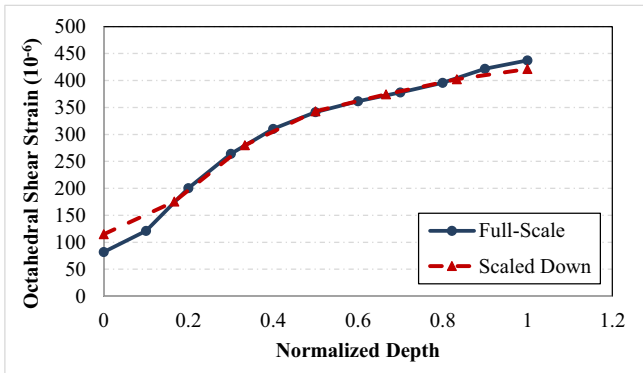
The full-scale model represents a pavement section comprising the asphalt, base, subbase, and subgrade layers. The thickness of the asphalt and base layers is 100 mm, whereas that of the subbase layer is 400 mm. The subgrade layer is modeled as an infinite layer. The full-scale FE model with element type C3D20R (a 20-node quadratic brick, reduced integration) for all layers is constructed in the quarter model by applying the symmetric boundary condition on the length and width direction according to the symmetric geometry. The loading pressure is considered 690 kPa. The asphalt concrete material is assumed to have two properties, elasticity and viscoelasticity, whereas the other layers are assumed to have elastic properties. The details of material properties are shown in Table 2.



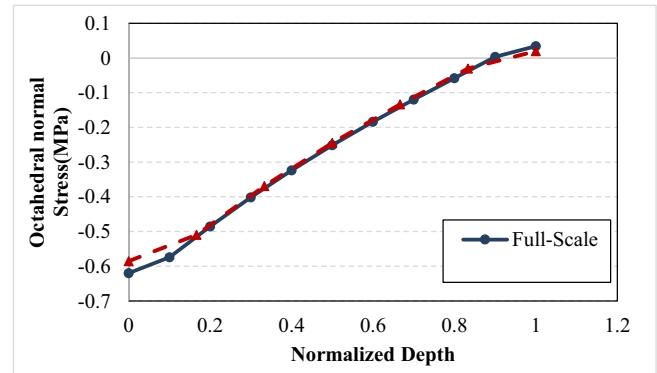
(a) Octahedral normal strain



(a) Octahedral normal stress



(b) Octahedral shear strain



(b) Octahedral shear stress

Fig. 3. Comparison of the octahedral (a) normal and (b) shear strains of the full-scale and scaled-down models at the center of model along with the normalized depth.

Fig. 4. Comparison of the octahedral (a) normal and (b) shear stresses of the full-scale and scaled-down models at the center of model along with the normalized depth.

3.1.1. Determination of contact area in the full-scale model

This study uses the real tire print to measure the actual tire-pavement contact area. The measured tire print is elliptical, and the geometry of the tire print can be modeled by a rectangle and two semicircles, as shown in Fig. 5(a). The length and width of the tire print can be denoted L and $0.6L$, respectively [17]. PCA (1984) simplified the real tire print into a rectangle with an equivalent area. The length and width of the rectangle are transformed to $0.8712L$ and $0.6L$, respectively, as shown in Fig. 5(b) [18]. The contact area A_C and length L can be derived using Eqs. (18) and (19), respectively. To model the element size conveniently, this study further simplified the aspect ratio to 3:2, as shown in Fig. 5(c). The error of the total contact area between two aspect ratios was less than 0.1%. The transformed length and width of the tire print were 210 and 140 mm, respectively, and the transformed contact area will be used in FE model to represent the tire contact area in full-scale model.

$$A_C = \pi(0.3L)^2 + (0.4L)(0.6L) = 0.5227L^2 \quad (18)$$

$$L = \sqrt{\frac{A_C}{0.5227}} \quad (19)$$

3.1.2. Determination of analysis domain for Full-Scale model

For efficient FE analysis, it is necessary to reduce the number of elements in the model without losing the accuracy of the calculation results. The sensitivity of the FE domain is analyzed by comparing the convergence of the octahedral strain between different FE domains to avoid boundary effects. The analysis considers the domain of the x - y plane and the finite domain of the subgrade in depth. The FE domain in the x - y plane is analyzed by comparing the cases with different ratios of the tire contact area, as demonstrated in Fig. 6. The element size is considered as $15 \times 14 \times 25 \text{ mm}^3$ for each FE model. Fig. 7 shows the comparison results for different FE domains in the x - y plane. The results show that increasing the FE analysis domain from 4 to 6 considerably affects the normal and shear octahedral strains. However, increasing the domain from 6 to 7 does not influence the octahedral strain considerably. Therefore, the FE domain in the x - y plane is set to six times the tire contact area. Fig. 8 shows the analysis results of the normal and shear octahedral strains of the finite FE domain in the subgrade layer. The results show that increasing the finite FE analysis domain in depth does not considerably affect the calculation results of the normal octahedral strain. Nevertheless, the octahedral shear strain

Table 2
Properties and thicknesses of typical provincial highways in Taiwan.

Pavement layer	Material type	Thickness (mm)	Material properties
Surface	Asphalt concrete	100	Elastic ($\nu = 0.3$; $E = 2070$ (MPa)) or Viscoelastic (Table 4)
Base	Asphalt treated base	100	$\nu = 0.35$; $E = 690$ (MPa)
Subbase	Crushed gravel	400	$\nu = 0.35$; $E = 180$ (MPa)
Subgrade	Soil	Infinite	$\nu = 0.45$; $E = 61.62$ (MPa)

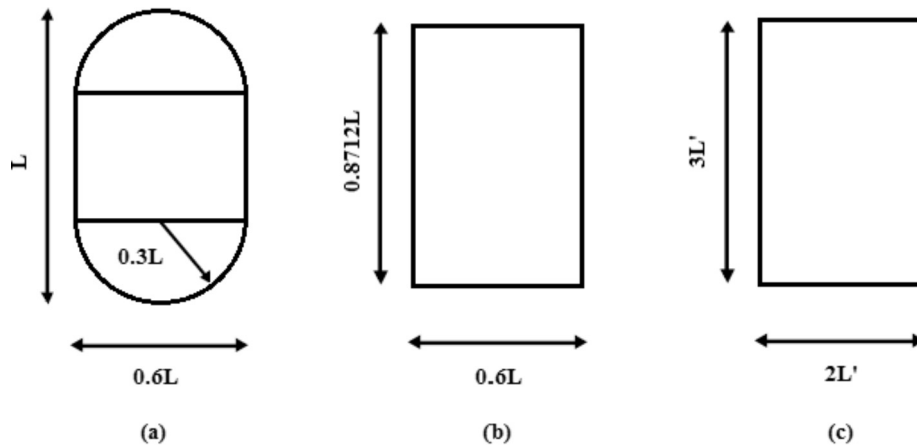


Fig. 5. (a) Real tire print (PCA, 1966), (b) simplified tire print (PCA, 1984), and (c) simplified tire print in this study.

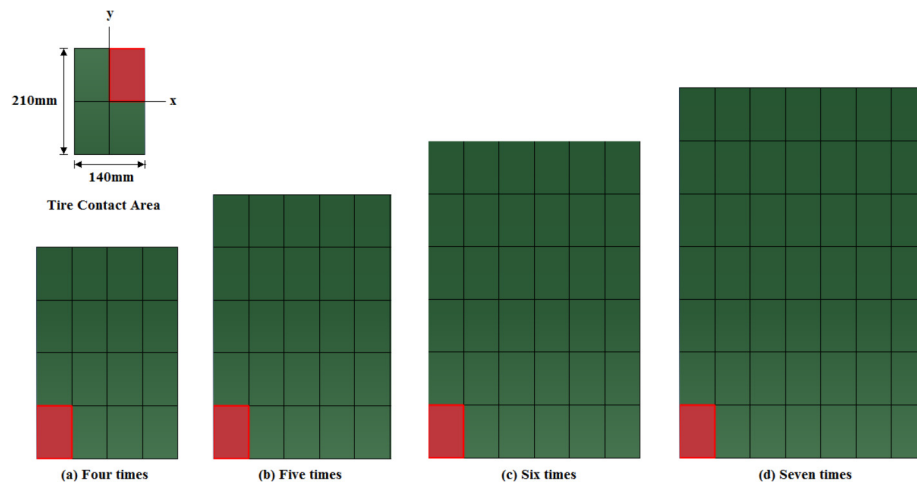


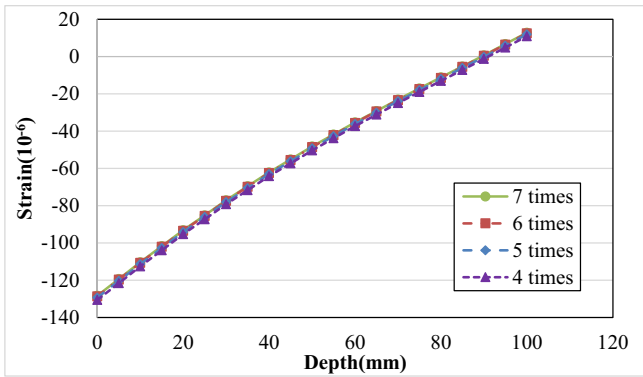
Fig. 6. Surface area of the quarter model for (a) four, (b) five, (c) six, and (d) seven times the length and width of the tire contact area.

changes with an increase in the finite FE domain from 500 to 600 mm, whereas the range from 600 to 700 mm does not affect the results considerably. Therefore, the finite FE range of the subgrade is selected as 600 mm in the full-scale model, which is shown in Fig. 9. The geometry of the quarter full-scale FE model has 420-mm in length, 630-mm in width and 1200-mm in depth.

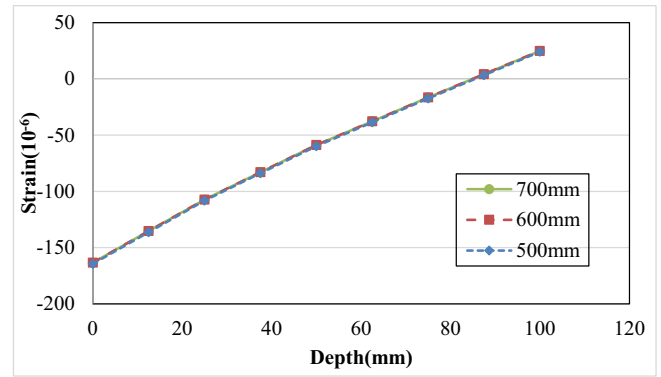
3.2. SALS FE model

Considering the workability and safety of the SALS facility in the laboratory, the scaled-down pavement system is designed as a two-layer system with asphalt and neoprene layers. The neoprene layer with 25 mm thickness rep-

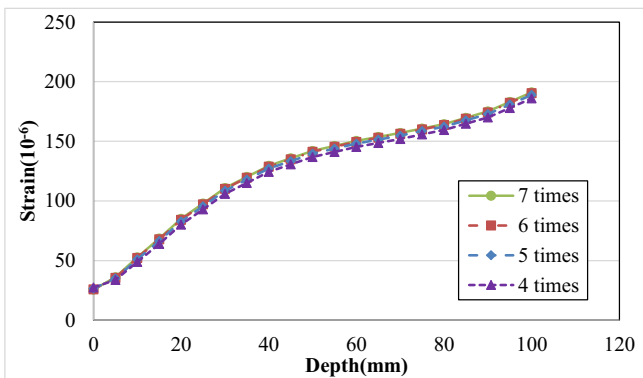
resents an equivalent layer of all layers underneath the asphalt layer in the full-scale pavement. Neoprene was used to model the supporting layers underneath the asphalt concrete surface and it is expected that the comparable deformation distribution of the full-scale and scaled down FE models can be achieved based on the theory of similitude. The dimensions of the asphalt concrete slab and neoprene layer were $800 \times 400 \text{ mm}^2$ in the tire-contact plane. According to the theory of similitude, the tire pressure is maintained at the same level as the pressure in the full-scale model, that is, 690 kPa, and the asphalt material properties are the same for both the full-scale and scaled-down models. The two-layer system (asphalt concrete slab and neoprene layer) is fixed by the precast cement concrete.



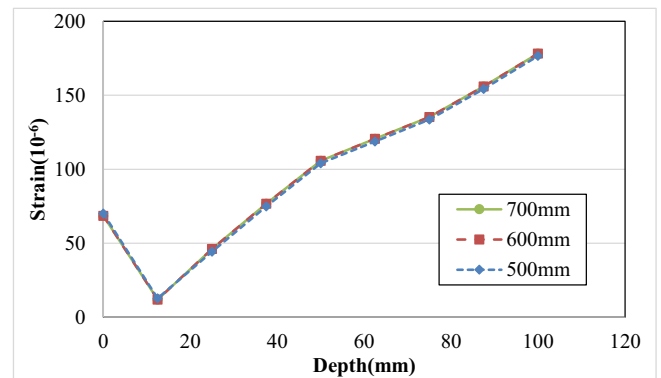
(a)



(a)



(b)



(b)

Fig. 7. Octahedral (a) normal and (b) shear strains of the full-scale 3D FE pavement model with different FE analysis range of x - y plane.

Fig. 8. Octahedral (a) normal and (b) shear strains of the full-scale 3D FE pavement model with different FE analysis range of subgrade finite depth.

Fig. 10 depicts the FE model of the SALS facility. The element type C3D20R is used for the asphalt material and C3D20RH (a 20-node quadratic brick, hybrid, linear pressure, reduced integration) is used for the neoprene material. Table 3 lists the material properties such as neoprene, steel and cement concrete of the SALS FE model, and the asphalt material properties is in Tables 2 and 4 for elastic and viscoelastic properties, respectively.

3.3. Development of the transfer functions (δ) between scaled-down and full-scale model according to FEA

This section presents FEA for developing the relationship between the full-scale pavement and scaled-down model for different scaling factors N . The asphalt material is considered elastic and viscoelastic in this study. Four cases of the scaled-down FE model with scaling factor $N = 0.9, 0.75, 0.6,$ and 0.45 are investigated. Subsequently, this study provides a method based on the time-temperature superposition principle for determining the optimal SALS testing temperature.

3.3.1. Elastic material under static loading

The simulation under static loading is implemented to investigate the vertical deformation of the asphalt layer

with elastic material property. The vertical deformation U_3 of the scaled-down model is denoted U_3^N . Fig. 11 shows the comparison of the vertical deformation within the asphalt concrete layer between the full-scale and scaled-down models. It is observed that the thicker the AC layer, the higher stiffness and the less deformation. Moreover, from Fig. 11, the deformation curve of the full-scale model could be represented by a vertical shift of the deformation curve of the scaled-down model. Therefore, a vertical shift factor δ_N^e can be obtained by minimizing the gap of vertical deformation between scaled-down and full-scale model. The vertical shift factor δ_N^e of various scaling factors N is shown in Fig. 12. A linear relationship can be observed between the scaling factor and the shift factors. The relationship between the full-scale and different scaled-down models can be expressed using Eq. (20). Fig. 13 shows that the U_3 distribution of the scaled-down model with vertical shifting δ_N^e can represent the vertical deformation of the full-scale model. The errors between the full-scale and scaled-down models after shifting were less than 0.63%.

$$F_i = \frac{S_{N_i}}{N} + \delta_N^e \tag{20}$$

where F_i is the U_3 of the full-scale model and S_{N_i} is the U_3 of the scaled down model with scaling factor N , the sub-

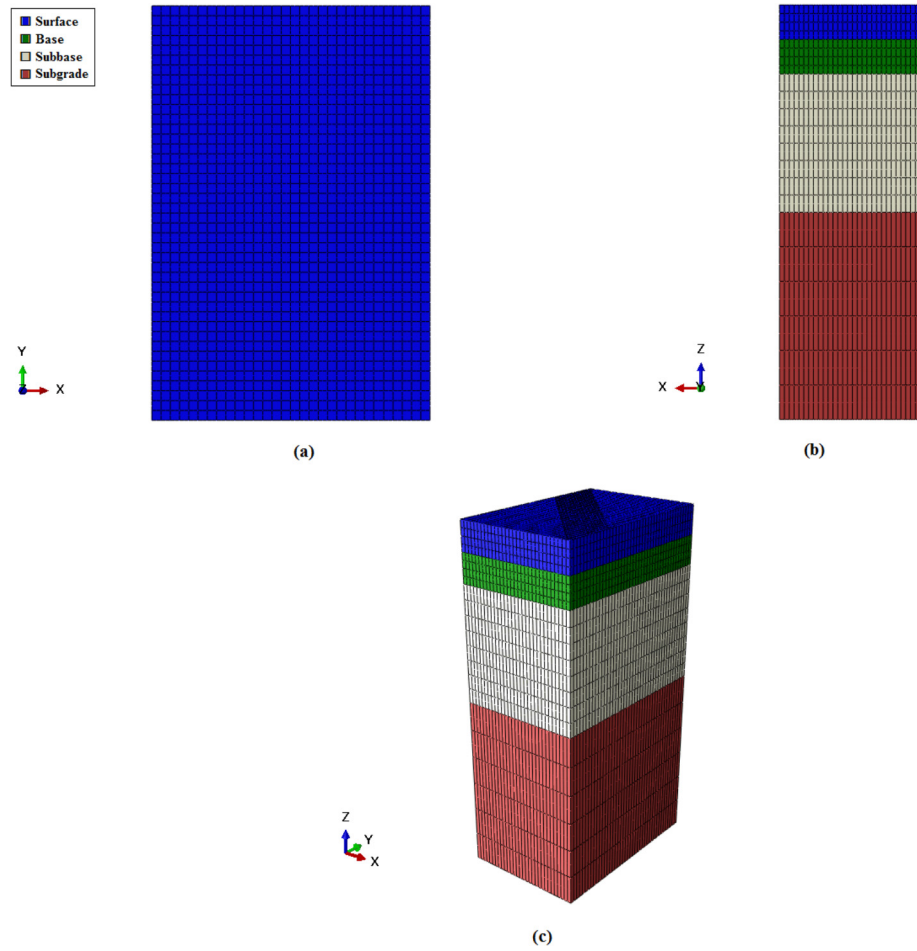


Fig. 9. Full-scale FE pavement model in (a) plane, (b) cross, and (c) 3D views.

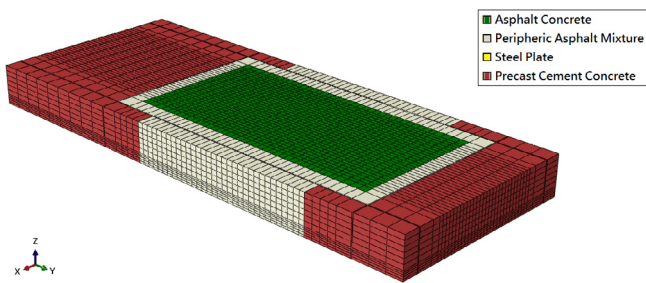


Fig. 10. Schematic of the 3D scaled-down FE model.

Table 3
Properties of the SALS's setup material.

Hyperelastic behavior		
	Quality	Hardness (Shore A)
Neoprene	C60	60 Shore
Elastic Behavior		
	Young's modulus (GPa)	Poisson's ratio
Steel	200	0.3
Cement Concrete	20	0.2

Table 4
Parameters of the Prony series used in this study.

n	Coefficient of Prony series D_n (1/MPa)	Retardation time λ_n (s)
1	4.53398E-05	0.001
2	2.22757E-05	0.01
3	4.20462E-05	0.1
4	0.000155018	1
5	9.31608E-05	10
6	0.000184771	100

$D_0 = 1.56956E-05$

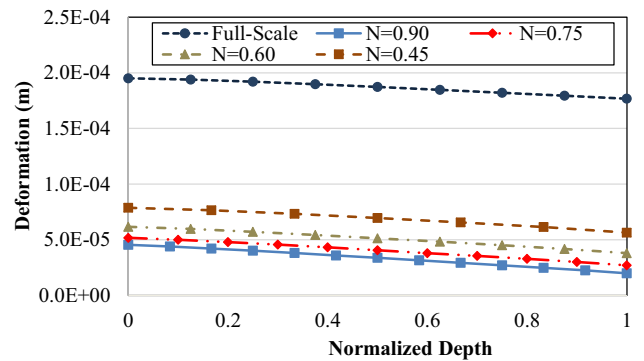


Fig. 11. U_3^N of the scaled-down models along the normalized depth.

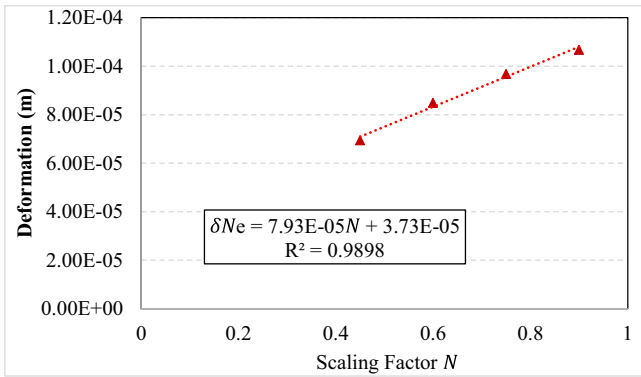


Fig. 12. Elastic shift factor δ_N^e of each scaling factor N .

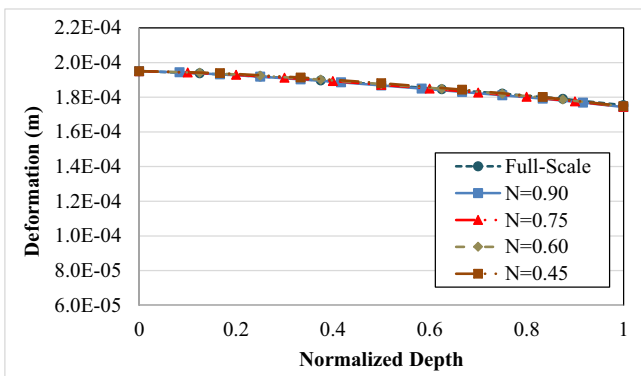


Fig. 13. U_3^N distribution of the full-scale and scaled-down FE models with the elastic shift factor δ_N^e along the normalized depth.

script i is the location of the variable within the layer. For example, $i = 0$ represents the variable on the top of the surface.

3.3.2. Viscoelastic material under step loading

According to the measurements of the asphalt material under an applied load, the asphalt material response is time-dependent. Therefore, the viscoelastic properties of the asphalt concrete layer were employed to further compare the full-scale pavement and scaled-down model. By applying a stress σ , the viscoelastic strain can be represented by Eq. (21).

$$\varepsilon(t) = \sigma D(t) \tag{21}$$

where σ is the applied stress and $D(t)$ is the creep compliance in time domain. The Boltzmann superposition principle calculates the response of complex loading histories for linear viscoelastic materials. The mathematical formulation of viscoelastic behavior is derived on the basis of the Boltzmann principle. The generalized form is expressed by Eq. (22), and the reduced time ψ^t is formulated using Eq. (23).

$$\varepsilon(t) = D_0 \sigma^t + \int_{-\infty}^t \Delta D(\psi^t - \psi^\tau) \frac{d(\sigma^t)}{d\tau} d\tau \tag{22}$$

$$\psi^t = \int_0^t \frac{d\xi}{a_T} \tag{23}$$

where D_0 and ΔD are the instantaneous elastic and transient compliances, respectively, and a_T is the time-temperature shift factor. The transient compliance ΔD is described using the Prony series, as shown in Eq. (24).

$$\Delta D^{\psi^t} = \sum_{n=1}^N D_n (1 - e^{-\lambda_n \psi^t}) \tag{24}$$

where D_n and λ_n are the n^{th} coefficient of the Prony series and retardation time, respectively.

According to AASHTO T342-11 test standard, the dynamic modulus test for asphalt concrete was conducted at five temperatures (5, 15, 25, 40, and 55 °C) and six loading frequencies (25, 10, 5, 1, 0.5, and 0.1 Hz); the diameter and height of the asphalt concrete sample were 10 and 15 cm, respectively [19]. The measurements of dynamic modulus D^* are shown in Fig. 14. The master curve is obtained through the horizontal shifting of the curves at different temperatures to the curve at the reference temperature according to time-temperature superposition principle. Fig. 15 shows the master curve in frequency domain, and Fig. 16 shows the relationship between the time-temperature shift factor and temperature. The measurements of dynamic modulus $|D^*|$ and phase angle δ are employed to calculate the storage modulus $D' = |D^*| \sin \delta$ and loss modulus $D'' = |D^*| \cos \delta$. Then, the Prony series shown in Eq. (25) is used to fit each the experimental measurements.

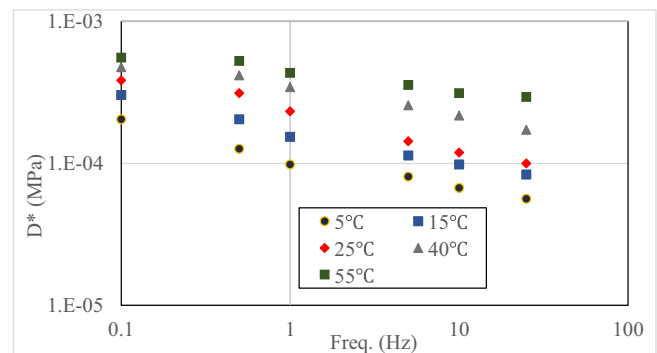


Fig. 14. Dynamic compliance D^* at each temperature.

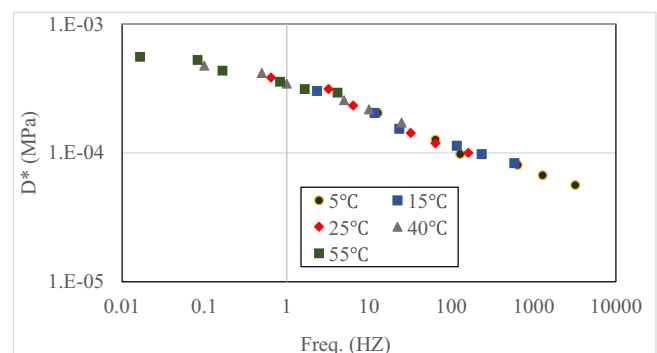


Fig. 15. Master curve of the dynamic compliance D^* of the asphalt concrete at a reference temperature of 25 °C.

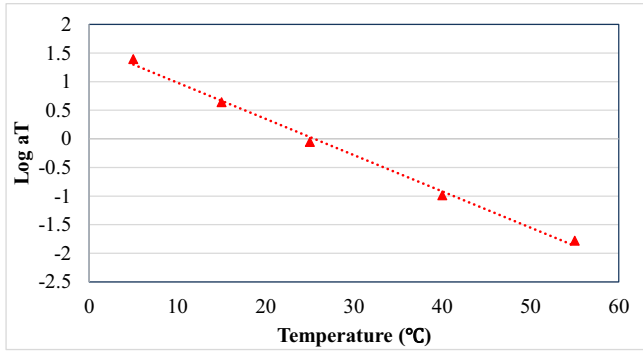


Fig. 16. Temperature shift factor a_T in the logarithmic scale.

The error function shown in Eq. (26) is minimized to fit the data.

$$D'(\omega) = D_0 + \sum_{n=1}^N \frac{D_N}{(\tau_n \omega)^2 + 1} \tag{25}$$

$$D''(\omega) = \sum_{n=1}^N \frac{D_i(\tau_n \omega)}{(\tau_n \omega)^2 + 1}$$

$$ERR = \left[\frac{D'_{model}}{D'_{exp}} - 1 \right]^2 + \left[\frac{D''_{model}}{D''_{exp}} - 1 \right]^2 \tag{26}$$

Once the Prony series coefficients are determined in the frequency domain, the series is formulated in terms of compliance as a function of time as in Eq. (24). The Prony series coefficients in Eq. (24) are listed in Table 4. These coefficients are the inputs in the FE analysis to simulate the viscoelastic behavior of the asphalt layer. This study uses the Pavement Analysis Using Nonlinear Damage Approach (PANDA) user material subroutine developed in the Advanced Research Consortium (ARC) project of the Texas A&M University research team to simulate the viscoelastic material behavior.

Because the material is time-dependent, the loading simulation must consider the time effect such as moving loading. However, the simulation of accurate moving loading is time-consuming. To overcome this difficulty, this study employs a strip loading with an equivalent loading time approach. The strip loading is a simplified representation of the moving loading path, and the equivalent loading time approach is mounted each loading pass duration to a continuous time span [14]. Fig. 17 presents the schematic of the simulated loading assumptions.

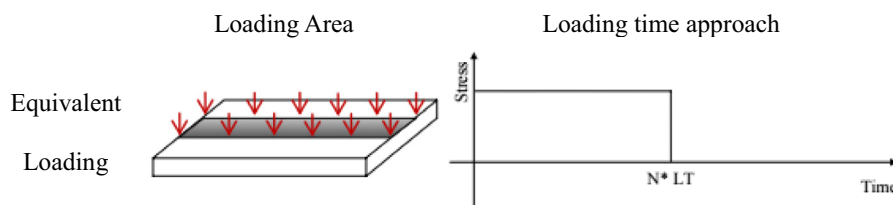


Fig. 17. Schematic of the simulated loading assumptions [14].

The trafficking in the full-scale model is simulated at 60 km/h. However, the maximum loading velocity of the SALS is 1.25 km/h, which is considerably slower than the desired loading velocity. The difference in loading history between the full-scale and scaled-down models considerably affects the asphalt material viscoelastic response. To consider this difference, this study employs the time-temperature superposition principle, which states that the asphalt material response at a loading frequency (loading speed) and temperature can be represented by another loading frequency at a specific temperature through time-temperature shifting. Losa and Natale et al. [15] and Mollenhauer et al. [16] have investigated the pulse spectrum of the strain induced by a traffic load. When a load moves over the pavement at a constant loading speed and temperature, the pavement exhibits a certain strain pulse frequency spectrum, as shown in Fig. 18. The loading speeds are determined for the full-scale and scaled-down models in this study, and the simulated temperature of the full-scale model is set as 50 °C. Therefore, a temperature for the scaled-down model is expected to be determined such that the material properties of the scaled-down model are equivalent to that of the full-scale model. Fig. 19 shows the schematic of this approach. The frequency f_F and temperature T_F in the full-scale model can be determined, and the modulus of the asphalt material is then obtained from the experimental measurement shown in Fig. 15. The testing temperature T_s of the scaled-down model can be determined through time-temperature shift-

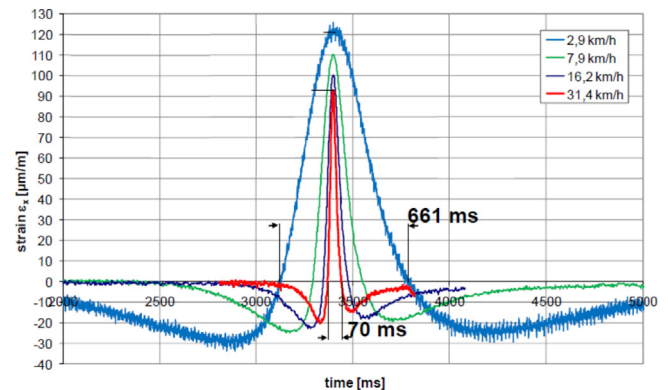


Fig. 18. Asphalt strains with respect to time induced by a 3500-kg static wheel load for various loading velocities [15].

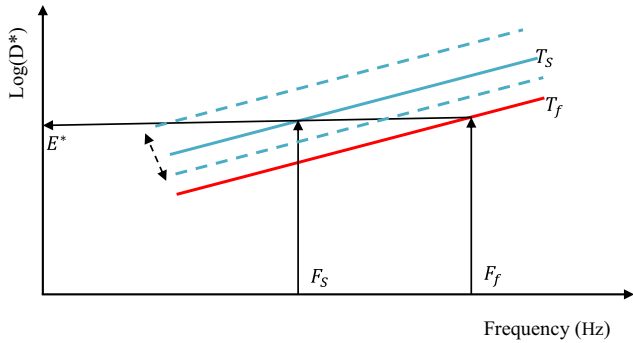


Fig. 19. Schematic of the approach for the scaled-down model to achieve identical material behavior of the full-scale model.

ing to the same modulus with the scaled-down loading frequency f_s . A systematic approach was adopted as follows to determine the test temperature of scaled-down model.

1. Develop the dynamic modulus master curve ($DMMC_{F-T}$) for pavement service temperature (T_F) of the full-scale pavement scenario (e.g., 50 °C).
2. Calculate the representative loading frequency of the full-scale pavement scenario $f_F = f(V_F, T_F)$.
3. Identify modulus stiff of the full-scale pavement scenario $E_F = E(f_F)$ at the corresponding representative loading frequency from dynamic modulus master curve.
4. Select the trial test temperature T_i for SALS test.
5. Develop the dynamic modulus master curve ($DMMC_{S-T_i}$) for testing temperature of the SALS (T_i).
6. Calculate the representative loading frequency of the SALS pavement scenario $f_S = f(V_S, T_i)$.
7. Identify modulus stiff of the SALS pavement scenario $E_S = E(f_S)$ at the corresponding representative loading frequency from dynamic modulus master curve.
8. Repeat step 5 to step 7 to minimizing the difference between E_F and E_S to obtain the optimized scaled-down model testing temperature T_i .

By employing the aforementioned procedure, the temperature of the scaled-down model is determined to be 20 °C. After the viscoelastic properties, loading types, and temperature of the full-scale and scaled-down models are determined, the two models can be compared through numerical simulation.

Figs. 20 and 21 show the contours of the vertical deformation U_3 between the full-scale and scaled-down FE models subjected to 1000 cycles of an equivalent strip load. A similar distribution was observed between the full-scale and scaled-down models. The highest compressive deformed areas were observed under the tire loading areas, and the tensile deformation (the heave) occurred along the side of the strip load, as observed in the field pavement. In addition, the deformation distribution in the lower scaling factor models was wider than that in the higher scaling factor models.

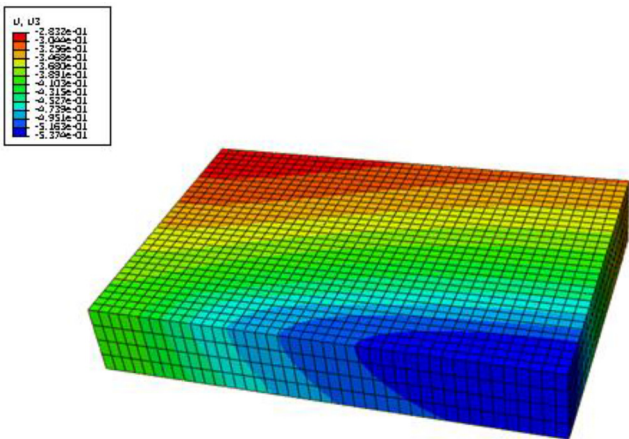


Fig. 20. U_3 (mm) contours of the full-scale FE quarter model after being subjected to 1000 cycles of an equivalent strip load.

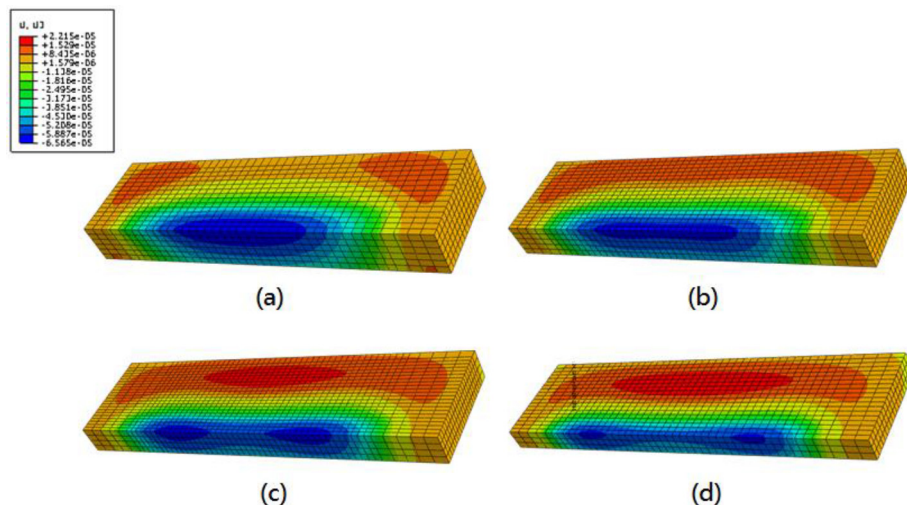


Fig. 21. U_3 (m) contours of (a) $N = 0.9$, (b) $N = 0.75$, (c) $N = 0.6$, and (d) $N = 0.45$ of the scaled-down models after being subjected to 1000 cycles of the equivalent strip load.

Fig. 22 shows the comparison between the scaled-down and full-scale models. The results show that a gap exists between the vertical deformations U_3 of the full-scale model and U_3^N of the scaled-down model. Fig. 23 shows the difference between $\log(U_3)$ and $\log(U_3^N)$. The difference in the vertical deformations between the full and scaled-down models has an approximated logarithmic trend-line, and the difference in the vertical deformation for each scaling factor N can be applied through a vertical shift δ_N^{ve} . Therefore, the viscoelastic shift factor δ_N^{ve} for each scaling is calculated similarly to the elastic shift factor δ_N^e ; Fig. 24 presents the

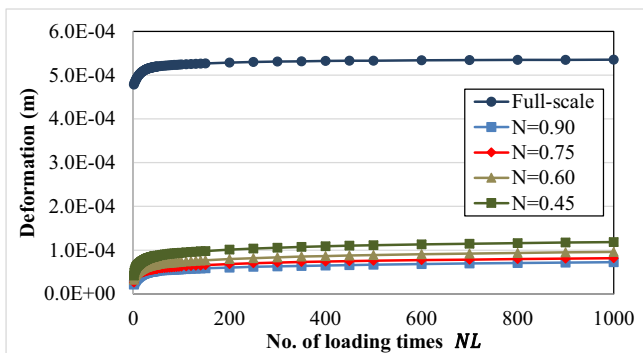


Fig. 22. U_3 of the full-scale model and U_3^N of the scaled-down model with adapted neoprene thickness with respect to the number of loading N_L .

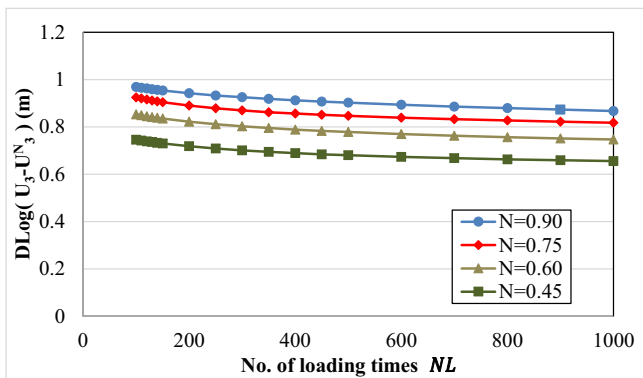


Fig. 23. Difference between the $\log U_3$ of the full-scale model and the $\log U_3^N$ of the scaled-down model with respect to the number of loading N_L .

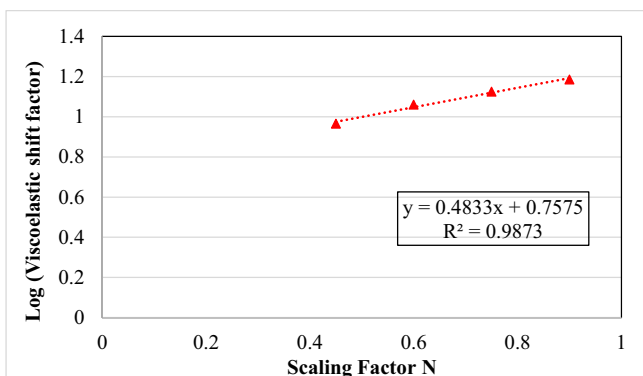


Fig. 24. Viscoelastic shift factor δ_N^{ve} of each scaling factor N .

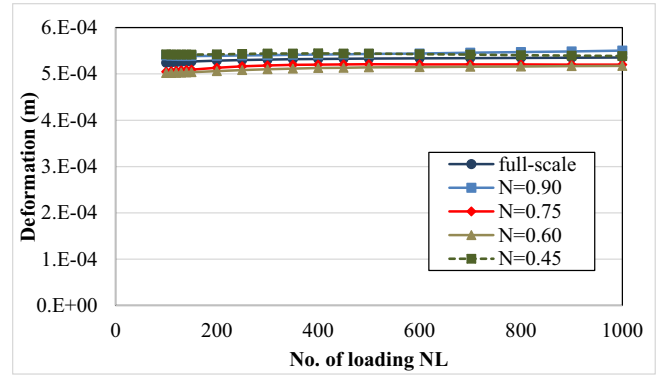


Fig. 25. U_3^N of the scaled-down model with the optimal neoprene thickness H_N after applying the viscoelastic shift factor δ_N^{ve} .

results of the viscoelastic shift factor δ_N^{ve} and scaling factor. The relationship between the U_3 of the full-scale model and the U_3^N of each scaled-down model is derived, as shown in Eq. (26). The vertical shift factor δ_N^{ve} can be calculated using a regressive equation, as shown in Fig. 24.

$$\log F_i = \log \frac{S_{N_i}}{N} + 0.0445 \ln N_L + \delta_N^{ve} \quad (27)$$

where N_L is the number of loading. Fig. 25 shows the result of the U_3^N for each scaling after shifting. The results show a good agreement between the variables of the full-scale and scaled-down models; the average error between the models after shifting is approximately 2.8%, and the maxima error is approximately 6%.

4. Conclusion

An analysis procedure for determining the relationship between the scaled-down pavement structure and the full-scale pavement structure was presented. The theory of similitude is validated by comparing the FEA between the scaled-down and full-scale models for a two-layer system. The results show that the theory can be used to efficiently scale down a full-scale model with the same number of layers and boundary condition. However, considering the ease of developing the SALS in the laboratory, completely scaling down the full pavement section is difficult. Therefore, this study employs the theory of similitude to determine the applied pressure, material properties, and conversion of the vertical deformation between the full-scale and scaled-down models. A full-scale FE model is developed to represent a complete section of the pavement structure, whereas the SALS facility is modeled using a scaled-down finite element model. The calculated vertical deformations are used to investigate the relationship between the SALS and the pavement section. Two properties of the asphalt material, elasticity and viscoelasticity, are considered. The results reveal that the vertical deformation in the scaled-down model can be shifted to that in the full-scale model for both elastic and viscoelastic materials.

The equivalent surface deformation of the full-scale model can be achieved by adapting the various neoprene

thickness and the shifting factors based on the vertical deformations. The result shows that the combination of optimal neoprene thickness H_N and shift factor of each scaled down models varies linearly with respect to scaling factor from 0.90 to 0.45. From the result of the research, the scaling $N = 0.75$ was employed for the SALS test configuration. Since with the scale, the 75 mm asphalt concrete slab is easy to construct in the laboratory and the 25 mm neoprene is commercially available.

Moreover, the loading simulation in this study is assumed as a strip loading with an accumulation loading duration. More realistic loading simulations, such as moving-loading simulation, will be performed in the future research.

References

- [1] National Cooperative Highway Research Program (NCHRP) 1-37A, Guide for Mechanistic-empirical Design of New and Rehabilitated Pavement Structures, 2004.
- [2] J.T. Harvey, CALTRANS Accelerated Pavement Test (CAL/APT) Program-Test Results: 1994–1997, 1998.
- [3] J. Groenendijk, A. Miradi, A.A.A. Molenaar, C.H. Vogelzang, L. Dohmen, A.M. Maagdenberg, M. DE BEER, Pavement Performance Modelling Using Lintrack, 1997.
- [4] F. Hugo, K. Fults, D. Chen, A.D.F. Smit, J. Bilyeu, An Overview of the TxMLS Program and Lessons Learned, Austin, Texas, 2000.
- [5] M.F.C. Van De Ven, D.F. Smit, The Role of the MMLS Devices in APT, no. July, pp. 17–20, 2000.
- [6] T. White, S.-M. Kim, F. Hugo, J.M. Roesset, Dimensional Analysis of the Model Mobile Load Simulator Action on Pavements, 1995.
- [7] A.L. Epps, T. Ahmed, D.C. Little, Fred Hugo, Performance Prediction with the MMLS3 at Westrack, FHWA, TX-01, 2134–1, 2001.
- [8] G.J. Simitzes, Structural similitude for flat laminated surfaces, *Compos. Struct.* 51 (2) (2001) 191–194, [https://doi.org/10.1016/S0263-8223\(00\)00144-6](https://doi.org/10.1016/S0263-8223(00)00144-6).
- [9] J. Rezaeepazhand, G.J. Simitzes, J.H. Starnes Jr., Use of scaled-down models for predicting vibration response of laminated plates, *Compos. Struct.* 30 (4) (1995) 419–426, [https://doi.org/10.1016/0263-8223\(94\)00064-6](https://doi.org/10.1016/0263-8223(94)00064-6).
- [10] J. Rezaeepazhand, G.J. Simitzes, J.H. Starnes Jr., Design of scaled down models for predicting shell vibration response, *J. Sound Vibr.* 195 (2) (1996) 301–311, <https://doi.org/10.1177/0954410015590637>.
- [11] M. Ramu, P.R.V. P.R. Thyla, Development of Structural Similitude and Scaling Laws for Elastic Models, 2010, pp. 67–69.
- [12] S. Bhattacharjee, J.S. Gould, R.B. Mallick, F. Hugo, An evaluation of use of accelerated loading equipment for determination of fatigue performance of asphalt pavement in laboratory, *Int. J. Pavement Eng.* 5 (2) (2004) 61–79, <https://doi.org/10.1080/10298430412331312472>.
- [13] F.H. Martin van de Ven, André de Fortier Smit, K. Jenkins, Scaled Down APT Considerations for Viscoelastic Materials, , 1998, pp. 602–615 (14).
- [14] R.K. Abu Al-Rub, M.K. Darabi, C.-W. Huang, E.A. Masad, D.N. Little, Comparing finite element and constitutive modelling techniques for predicting rutting of asphalt pavements, *Int. J. Pavement Eng.* 13 (4) (2012) 322–338, <https://doi.org/10.1080/10298436.2011.566613>.
- [15] M. Losa, A. Natale, Evaluation of representative loading frequency for linear elastic analysis of asphalt pavements, *Transp. Res. Rec. J. Transp. Res. Board* 2305 (2012) 150–161, <https://doi.org/10.3141/2305-16>.
- [16] K. Mollenhauer, M. Wistuba, R. Rabe, Loading Frequency and Fatigue; In situ Conditions & Impact on Test Results, 2009, pp. 261–276.
- [17] Portland Cement Association (PCA), Thickness Design for Concrete Pavements, Portland Cement Association, Skokie, IL, 1996.
- [18] Portland Cement Association (PCA), Thickness Design for Concrete Highway and Street Pavements, Engineering Bulletin EB 109P, Portland Cement Association, Skokie, IL, 1984.
- [19] AASHTO, T342, Standard Method of Test for Determining the Dynamic Modulus and Flow Number for Hot Mix Asphalt (HMA), American Association of State Highway and Transportation Officials, Washington, DC, 2015.